Title	Visible laser scribing fabrication of porous graphitic carbon electrodes: Morphology, electrochemical properties and applications as disposable sensor platform
Authors	Vaughan, Eoghan;Larrigy, Cathal;Burke, Micheal;Sygellou, Labrini;Quinn, Aidan J.;Galiotis, Costas;Iacopino, Daniela
Publication date	2020-09-23
Original Citation	Vaughan, E., Larrigy, C., Burke, M., Sygellou, L., Quinn, A. J., Galiotis, C. and Iacopino, D (2020) 'Visible laser scribing fabrication of porous graphitic carbon electrodes: Morphology, electrochemical properties and applications as disposable sensor platform', ACS Applied Electronic Materials. doi: 10.1021/acsaelm.0c00612
Type of publication	Article (peer-reviewed)
Link to publisher's version	10.1021/acsaelm.0c00612
Rights	© 2020, American Chemical Society. This document is the Accepted Manuscript version of a Published Work that appeared in final form in ACS Applied Electronic Materials, after technical editing by the publisher. To access the final edited and published work see https://pubs.acs.org/doi/abs/10.1021/acsaelm.0c00612
Download date	2024-11-24 05:10:46
Item downloaded from	https://hdl.handle.net/10468/10610

ACS APPLIED ELECTRONIC MATERIALS

Article

Visible Laser Scribing Fabrication of Porous Graphitic Carbon Electrodes: Morphology, Electrochemical Properties and Applications as Disposable Sensor Platform

Eoghan Vaughan, Cathal Larrigy, Micheal Burke, Labrini Sygellou, Aidan J. Quinn, Costas Galiotis, and Daniela Iacopino

ACS Appl. Electron. Mater., **Just Accepted Manuscript** • DOI: 10.1021/acsaelm.0c00612 • Publication Date (Web): 23 Sep 2020

Just Accepted

is published by the American Chemical Society. 1155 Sixteenth Street N.W., Washington, DC 20036

Visible Laser Scribing Fabrication of Porous Graphitic Carbon Electrodes: Morphology, Electrochemical Properties and Applications as Disposable Sensor Platform

*Eoghan Vaughan,[a] Cathal Larrigy,[a] Micheal Burke,[a] Labrini Sygellou,[b] Aidan J. Quinn,[a] Costas Galiotis,[b,c] Daniela Iacopino[a]**

[a]Tyndall National Institute, University College Cork, Dyke Parade, Cork, Ireland

[b]Institute of Chemical Engineering Sciences, Foundation for Research and Technology-Hellas (FORTH/ICE-HT), Patras 265 04, Greece

[c]Department of Chemical Engineering, University of Patras, Patras 26504, Greece

KEYWORDS Direct laser writing, graphitic carbon, Laser Induced Graphene, electrochemical sensors, ascorbic acid, uric acid, dopamine.

ABSTRACT. Porous graphitic carbon electrodes were fabricated by laser scribing of commercial polyimide tape. The process was performed by a simple one-step procedure

using visible wavelength laser irradiation from a low-cost hobbyist laser cutter. The obtained electrodes displayed a highly porous morphology, rich in three-dimensional (3D) interconnected networks and edge planes, suitable for electrochemical sensing applications. Spectral characterization by Raman and XPS spectroscopies revealed a crystalline graphitic carbon structure with high percentage of sp^2 carbon bonds. Extensive electrochemical characterization performed with outer sphere $[Ru(NH_3)_6]^{3+}$ and inner sphere $[Fe(CN)_6]^{4-}$, $Fe^{2+/3+}$ and dopamine redox mediators showed quasi-reversible electron transfer at the graphitic carbon surface, mainly dominated by a mass diffusion process. Fast heterogeneous electron-transfer rates, higher than similar carbon-based materials and higher than other graphitic carbon electrodes produced by either visible or infrared laser irradiation, were obtained for these electrodes. Thin-layer transport mechanisms occurring in parallel to the main diffusion-limited mechanism were taken into consideration, but overall the observed enhanced electron-transfer rates effects were ascribed to the large specific surface area of the extended 3D porous network, rich in defects and edge-planes. The superior electrocatalytic properties of the fabricated electrodes allowed electrochemical differentiation between the biomarkers ascorbic acid,

dopamine and uric acid in solution. The compatibility of fabricated electrodes with light-weight portable and handheld instrumentation makes such electrodes highly promising for the realisation of low-cost disposable sensing platforms for point-of-care applications.

Introduction

The application of graphene and graphitic materials for use as electrochemical sensors has been extensively investigated due to their remarkable physical and chemical properties. Such materials possess a wide electrochemical window and exhibit electrocatalytic activity for many redox reactions.[1,2] Moreover, they possess a rich surface chemistry amenable to surface modification towards realisation of selective and sensitive biosensing platforms.[3,4] The electrochemical performance of graphitic materials is highly dependent on their morphology. For example, it has been reported that the presence of edge-planes facilitates rapid electron-transfer (ET), surface functional groups act as electrocatalytic sites, and the formation of extended 3D porous networks provide high-surface area electrodes and allows easy access for the electrolyte ions into the carbon material.[2, 5-8] Therefore, the ability to control the fabrication process and the resulting

morphology of graphitic materials is of key importance to tune, enhance and widen their performance as electrochemical sensors and biosensors. Standard fabrication processes of graphene-like materials such as chemical vapour deposition[9] or self-assembly of reduced graphene oxide[10] are often expensive and time-consuming. Other less cumbersome methods such as screen printing or inkjet printing require the use of binders or additives that might affect the electrochemical sensitivity of the resulting electrodes[11-14] whereas solution processing of graphene often results in aggregation and reduced surface area electrodes.[11]

Recently, direct laser writing techniques have been proposed as an alternative for the fabrication of disposable electrochemical sensors. In this technique, a light scribe-enabled disk drive is used for the patterning of graphene oxide on PET films pre-deposited on DVD surfaces.[15,16] Electrochemical sensors were fabricated displaying a fast heterogeneous electron transfer (HET) rate compared to commercial edge plane pyrolytic graphite (EPPG). However, the DVD scribing method required multistep chemical processing, each laser irradiation took 20 min to complete and had to be repeated 10 times to ensure reduction of graphene oxide, optimal expansion and acceptable

conductivity.[15] A further simplified technique was later proposed by Tour *et al.*[17, 18] In this method simple computer-aided laser-scribing techniques were used for the fabrication of graphitic carbon structures on commercial polyimide sheets (Kapton tape). The technique was based on the use of hobbyist-laser cutters and allowed fast patterning of a variety of electrode designs onto flexible Kapton tape by a simple one-step CO_2 laser irradiation under ambient conditions. The obtained graphitic carbon structures were characterized by high porosity and electrical conductivity and displayed spectral features associated to crystalline graphitic carbon structures[18] The graphitization of polyimide was ascribed to the high local temperature (> 2500 °C) induced by a resonance effect between the laser wavelength and the polyimide.[18,19] Nayak *et al.* investigated in detail the capability of such graphitic electrodes for on-chip electrochemical sensing and found that the morphology of the graphitic carbon, rich in defects, edge planes and surface functional groups was particularly suitable to electrochemical sensing applications.[19] Furthermore, a detailed study was recently performed by our group whereby the morphology of graphitic carbon electrodes fabricated with a low cost visible laser cutter (405 nm wavelength) was investigated at different laser dwell time per pixel.[20] Optimum experimental conditions led

to formation of highly porous structures displaying electrical and spectral characteristics comparable to equivalent graphitic carbon structures obtained with high cost CO_2 lasers. The electrodes displayed quasi-reversible behaviour with ΔE_P values of 74.5 mV and 85.6 mV obtained with $[Ru(NH_3)_6]^{3+/2+}$ and $[Fe(CN)_6]^{4-/3-}$ redox mediators, respectively. Also fast electron transfer rates were calculated equivalent to 0.0146 and 0.013 cm/s for $Ru(NH_3)_6]^{3+/2+}$ and $[Fe(CN)_6]^{3-/4-}$ redox mediators, respectively.

The biosensing performance of carbon-based electrodes is often tested by investigation of their electrochemical capabilities towards ascorbic acid (AA), dopamine (DA), and uric acid (UA) - both individually and in mixtures. AA plays a key role in biological metabolism, whereas DA and UA are important biomarkers for detection of neurological disorders and kidney diseases, respectively.[21-23] AA, DA and UA coexist in the central nervous system. However, their detection by electrochemical techniques is disabled in bulk electrodes by the overlapping of their oxidation potentials. Therefore, the simultaneous detection of AA, DA and UA in solution is an insightful experiment to determine the selectivity of a graphene-like biosensor. Graphitic carbon-based electrochemical sensors have shown high electro-catalytic activity, high sensitivity toward AA, DA, and UA and individual

component detection capabilities in AA/DA/UR mixtures.[19,24] However, such sensitivity has been achieved by enhancement of the electrocatalytic performance of the graphitic carbon electrodes by selective Pt deposition or conductive polymer PEDOT electrodeposition.[19,24]

In this paper, the formation of 3D graphitic carbon electrodes obtained by direct laser writing of polyimide substrates is presented. The graphitization of polyimide occurred under ambient conditions by irradiation with a low-cost laser cutter tool equipped with a 450 nm wavelength laser. Conductive, porous structures with high density of edge planes and displaying nanocrystalline graphitic carbon spectral signatures, evidenced by Raman and X-ray photoelectron spectroscopy (XPS) data were formed by simple one-step laser irradiation. Obtained electrodes were tested with inner-sphere and outer-sphere redox mediators and showed extremely fast HET rates, higher than other graphitic carbon structures obtained with visible and infrared laser engraving machines. The electrochemistry process was mainly diffusion limited. However, the occurrence of thin-layer voltammetric processes within the porous electrode was also investigated. Fabricated electrodes exhibited superior biosensor performance, allowing simultaneous

detection of AA, DA and UA mixtures, without any further modification of the electrode surface. The superior electrocatalytic properties were ascribed to the porous and extended 3D morphology of the graphitic carbon electrodes, rich in defects and edge planes.

Experimental session

Materials. Polyimide films with thickness of 80 μm were purchased from Radionics and used without further treatment. DA, UA and AA were purchased from Sigma Aldrich and used without further purification. The redox systems used were the following: $[Ru(NH_3)_6]^{3+}$ (5 mM) in KCl (1 M) from $[Ru(NH_3)_6]Cl_3$ (Sigma-Aldrich); $[Fe(CN)_6]^{4-}$ (5 mM) in KCl (1 M) from $K_4Fe(CN)_6$ (Sigma-Aldrich); $Fe^{2+/3+}$ (3 mM) in $HClO_4$ (0.1 M) made from $Fe(NH_4)_2(SO_4).12H_2O$ and $HClO_4$ (0.1 M); DA (1 mM) in $HClO_4$ (0.1 M). All solutions were prepared using deionized Milli-Q water (resistivity 18.2 MΩ.cm) and deoxygenated with N_2.

Electrode fabrication. Graphitic carbon electrodes were fabricated by raster scanning of designed electrode structures on polyimide by a KKmoon Compact Automatic Desktop Laser Engraving Machine equipped with a laser with 3 W power and illumination

wavelength of 450 nm.[20] A glass slide was used as a rigid substrate to support polyimide tape which was irradiated at 30% laser power. An acetone-isopropanol-DI water wash was applied to the electrodes before use to remove any residues from the laser engraving process.

Characterisation. The morphology of graphitic carbon electrodes was characterized by a cold-cathode field-emission Scanning Electron Microscope (SEM, JSM- 7500F, JEOL UK Ltd.) operating at 5 kV acceleration voltage. White light optical microscopy images of fabricated graphitic carbon electrodes were acquired with an Axioskop II, Carl Zeiss Ltd. Microscope interfaced to a charge-coupled detector camera (Coolsnap CF, Photometrics). Surface wettability was measured by a Dataphysics OCA 20 Wetting angle system in air at ambient temperature by dropping distilled water droplets (1 mm diameter) on the graphitic carbon surfaces. The average contact angle value was acquired by measuring at six different positions of the same sample. Raman measurements were performed with a Renishaw inVia Raman system equipped with a 514 nm helium–neon laser. The laser beam was focused onto the sample through a Leica 20X objective with 0.4 N.A. Acquisition time was usually 10 s and measured power was 3 mW. X-ray

photoelectron spectroscopy (XPS) measurements were carried out in an ultrahigh vacuum (UHV) chamber, with a base pressure ~$5x10^{-10}$ mbar, equipped with a SPECS LHS-10 hemispherical electron analyser and a dual anode Al/Mg x-ray gun. All XPS measurements were acquired using the un-monochromatized Mg Kα line at 1253.6 eV and an analyser pass energy of 36 eV, giving a full width at half maximum (FWHM) of 0.9 eV for the Au 4f7/2 peak. The XPS core level spectra were analysed by fitting each total spectrum to a series of individual mixed Gaussian-Lorentzian peaks following a Shirley background subtraction.

Electrochemical analysis. Cyclic voltammetry (CV) and Differential Pulse Voltammetry (DPV) electrochemical measurements were performed with a CHI760 bi-potentiostat and handheld EmStatblue (PalmSens) electrochemical systems using a Pt wire as counter electrode, Ag/AgCl as reference electrode and graphitic carbon as working electrode. The parameters for the DPV measurements were: 0.004 V increment; 0.05 V amplitude; 0.1 s pulse width; 0.01 s sample width; 0.5 s pulse period. The three electrodes were assembled in a Teflon cell with a circular area of 8 mm diameter exposed to the electrolyte. The electrochemical cell setup is shown in supporting information figure S5

(a) and (b). Electrolyte solutions were purged with N_2 for 30 min prior to measurements. Heterogeneous electron transfer (HET) rate constants were determined from the anodic/cathodic peak separation using the method of Nicholson[25] by assuming transfer coefficient α = 0.5 and using the following diffusion coefficients: $[Ru(NH3)_6]^{3+/2+}$ D_0 = 6.5 × 10^{-6} cm^2 s^{-1}; $[Fe(CN)_6]^{4-/3-}$ D_0 = 7.63 × 10^{-6} cm^2 s^{-1}, D_R = 6.32 × 10^{-6} cm^2 s^{-1}, $Fe^{2+/3+}$ D_0 = 7.9 × 10^{-6} cm^2 s^{-1}; dopamine D_0 = 6.0 × 10^{-6} cm^2 s^{-1}. In all cases except for $[Fe(CN)_6]^{4-/3-}$ it was assumed that $D_0 = D_R$.

Results and discussion

Morphological characterization

Figure 1a shows a scheme of the direct laser writing method used to fabricate graphitic carbon electrodes in this work. Figure 1b shows a white light optical image of a representative single electrode (18 mm in length) obtained by back and forth raster scanning of the visible laser on the polyimide surface. The electrode width measured at different points along the length was homogeneous with a mean value of 215 μm.

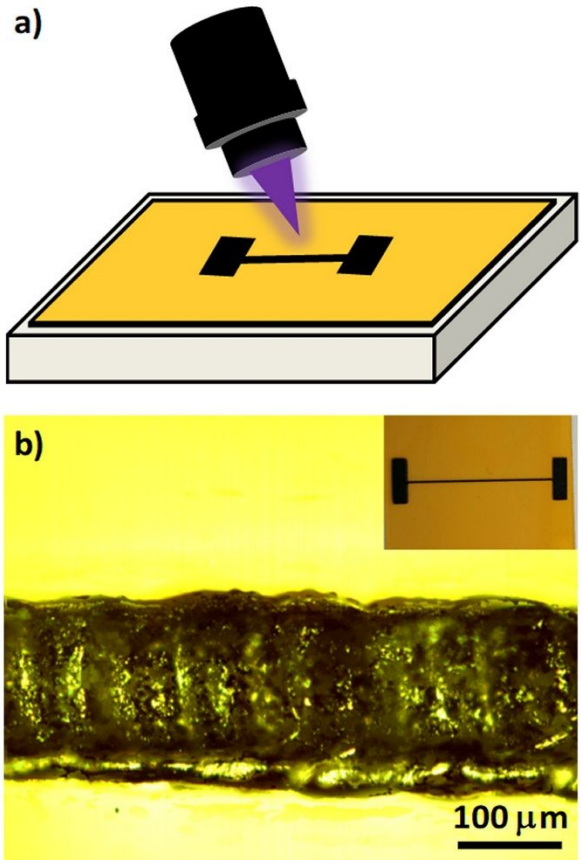

Figure 1. a) Schematic of the laser scribing method used for fabrication of graphitic carbon electrodes; b) representative white light optical image of a fabricated graphitic carbon electrode. Inset photograph showing the entire structure of a typical graphitic carbon working electrode.

Observation of the line microstructure by electron microscopy (Figure 2a) showed that the fabricated structural morphology was characterized by a quite regular and flaky structure displaying high porosity and high surface area, similar to the morphology of graphene-like carbon electrodes obtained with other laser wavelengths.[18, 20, 26-27] An extended 3D network of overlapped

graphitic carbon sheets with a high density of accessible edges constituted by kinked and wrinkled areas was also observable from the SEM images. The occurrence of a morphology displaying high density of "exploded" pores has already been reported for graphitic structures written either with visible or infrared laser illumination. The suggested mechanism for the conversion of polyimide to graphitic structures is the absorption of laser photon energy and conversion of this energy to heat resulting in localized high pressure and temperature conditions.[18,20] The presence of available oxygen and moisture, due to the process being performed in air, caused the ablation of some carbon, resulting in the observed porous structure. Such porous 3D morphology is expected to offer highly accessible electrochemical surface area, whereas the high density of edge planes is expected to enhance electrochemical transfer behavior, making these structures promising for electrochemical sensing applications. The characterization of the electrode surface by contact angle measurements (Figure 2b) revealed its hydrophilic nature. An average contact angle of 65.5° was measured, which should also enhance electrochemical sensing by facilitating efficient circulation of analytes into the porous surface. The Raman spectrum of the graphitic carbon electrode (Figure 2c) was characterized by three main peaks centered at 1351, 1584 and 2699 cm^{-1} corresponding to the so called D peak (induced by bent sp^2 carbon bonds and associated with the presence of defects), G peak (corresponding to the E2g vibration mode of graphitic carbon) and 2D peak, respectively. Also a minor peak at 2937 cm^{-1} was observed in this high wavelength part of the spectrum, corresponding to the D + D" peak. The presence of the above peaks clearly indicated the formation of a graphite-like carbon morphology. More specifically, the maximum in the *D* region could be fit with a single, sharp Lorentzian with full-width at half-maximum intensity, $FWHM(D) \sim 52$ cm^{-1}, consistent with low disorder. The other first-order peak represented a convolution of the *G* peak centered at 1575 cm^{-1} and a weaker *D*' peak centered at 1610 cm^{-1}.[28]. In early Raman studies

of graphite, *D*' peak signatures were observed in high-quality polycrystalline graphite and also by creating defects in natural graphite single crystals.[29,30] Casiraghi and co-workers established empirical relationships between the intensity ratio of the *D* and *D*' peaks, and the nature of the defects in natural graphite or deliberately created in exfoliated monolayer graphene.[31] They reported $I_D/I_{D'} \sim 7$ for vacancy defects, close to the $I_D/I_{D'} \sim 6$ reported in Figure 2c. The ratio $I_D/I_G \approx 1$ confirmed the crystalline nature of the ablated surface and was in agreement with formation of highly ordered graphite and nanocrystalline graphitic domains in a disordered carbon matrix;[20] the high I_{2D}/I_G ratio indicated a low number of graphene layers.[18, 20] Moreover, the 2D peak could be fitted by a single Lorentzian peak centered at 2699 cm^{-1}, with a FWHM of 71 cm^{-1}. This profile was consistent with 2D graphitic structures consisting of randomly stacked graphene layers along the c-axis, already reported by illumination of polyimide with high power infrared laser sources.[18] Figure 2d shows the deconvoluted C1s XPS peak for a measured graphitic carbon area. The peak was analyzed into five components (the main C-C sp^2 and C-C sp^3 carbon bonds, C-O(H) epoxides and hydroxides, C=O carbonyl groups, and COOH carboxyl groups and the $\pi-\pi^*$ transition loss). Peak assignments and percentage component concentrations are shown in Table 1. XPS data showed that the majority of the polyimide film was converted into sp^2 carbon (71.07%), further confirming the graphene-like nature of the obtained structure. Moreover, close observation of the XPS percentage atomic concentration for nitrogen (see Figure S1) revealed low concentration of N1s (2.45 %), further confirming the conversion of polyimide into graphitic carbon. Also confirmed was the presence of surface carboxyl and carbonyl groups with C-O peak more dominant than C=O peak (13.08 vs 4.03 %, respectively). It has been reported that the presence of oxygen functional groups at the surface of graphene electrodes should promote increased electrocatalytic activity and an increase in the HET rate.[32,33]

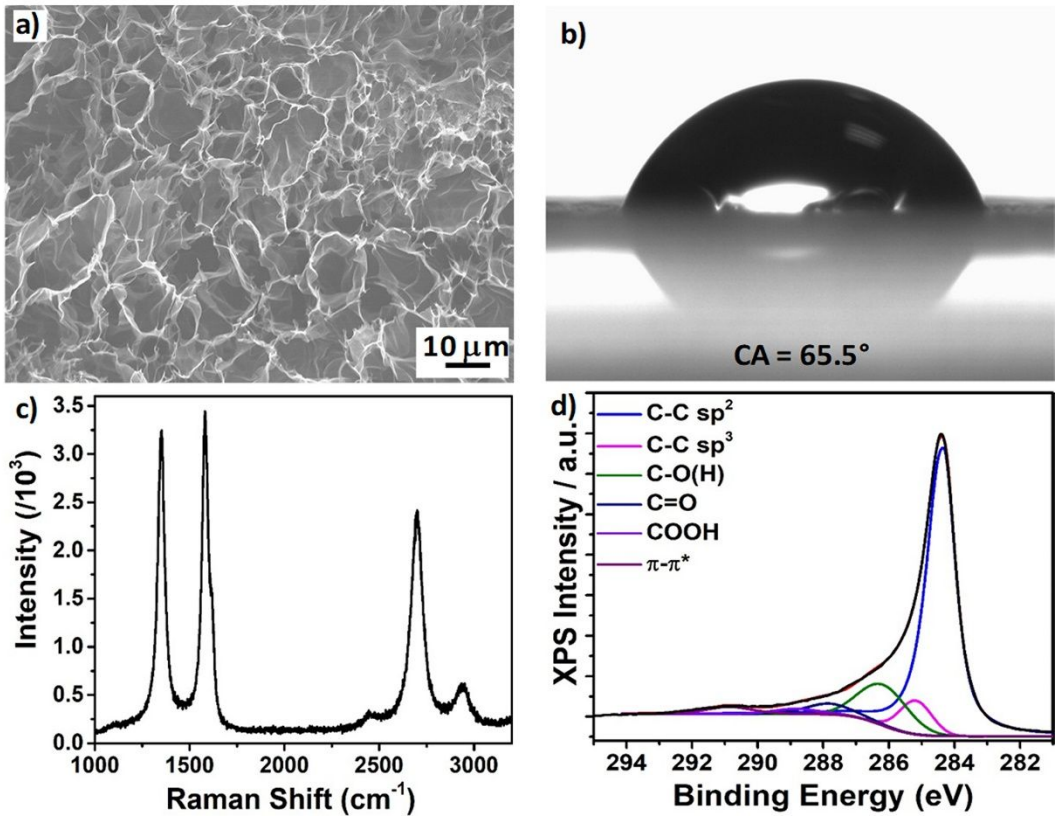

Figure 2. a) SEM image of a typical graphitic carbon electrode; b) contact angle measurement at the graphitic carbon surface; c) Raman spectrum and d) XPS spectrum of graphitic carbon electrodes.

Table 1. Percentage carbon component concentration derived from the XPS C1s peak deconvolution

Binding energy (eV)	Atomic percentage (%)	Assignments
284.33	71.07 ± 0.14	C-C sp^2
285.18	7.16 ± 0.12	C-C sp^3
286.18	13.08 ± 0.08	C-O(H)
287.83	4.03 ± 0.06	C=O
288.83	1.96 ± 0.06	COOH
290.88	2.70 ± 0.05	π-π* transition

Electrochemical characterization

In order to fully investigate the electrochemical behaviour of the fabricated graphitic carbon electrodes the following redox systems were selected: $[Ru(NH_3)_6]^{3+/2+}$, $[Fe(CN)_6]^{3-/4-}$, $Fe^{3+/2+}$ and DA, in order to gain insights on the material electronic properties, surface microstructure and surface chemistry. For each system, the heterogeneous electron transfer (HET) rate constant, k^0_{app}, was calculated using the Nicholson method.[25] Figure 3a shows CVs of the outer sphere redox mediator $[Ru(NH_3)_6]^{3+/2+}$ recorded in the 100 - 1000 mV/s scan rate range. The formal potential for this couple (CV $E_{1/2}$ value) was -0.175 V. As the $[Ru(NH_3)_6]^{3+/2+}$ redox couple is insensitive to the surface microstructure, surface oxides and adsorbed monolayers on sp^2 carbon electrodes, the main factor affecting the reaction rate was the availability of electronic states (density of electronic states, DoS) near the formal potential of the redox system.[1,34-35] The average ΔE_P

calculated at 100 mV/s scan rate over three electrodes was found 57 mV (σ = 4.2 mV), below the theoretical minimum peak separation of 59 mV for a one-electron reversible reaction. Using the Nicholson method, a value of k^0_{app} of 6.9×10^{-2} cm/s was determined for this redox system (see details of calculations in Figure S2a). This k^0_{app} value was 5 times higher than the value previously obtained by our group for graphitic carbon electrodes obtained with 405 nm laser cutters.[20] The extremely low peak separation and rapid electron transfer rate suggested a high DoS for the system near the formal potential of $[Ru(NH_3)_6]^{3+/2+}$. It should be pointed out that the ΔE_P value found for this system was 1.3 and 1.5 times lower than the value previously obtained by our group and others for porous graphitic carbon electrodes obtained with 405 nm and 10.6 mm irradiation wavelengths.[19,20]

Further exploration of the nature of this low value for the peak-to-peak separation will be discussed later. The electrochemical behaviour measured in the 100 -1000 mV/s scan rate range showed quasi-reversible behaviour, shown by the linear relationship between the peak oxidation/reduction current and the square root of the scan rate (inset of Figure

3a) and indicating a semi-infinite linear diffusion reaction process (with correlation coefficients for oxidation and reduction processes equal to 0.996 and 0.995, respectively).

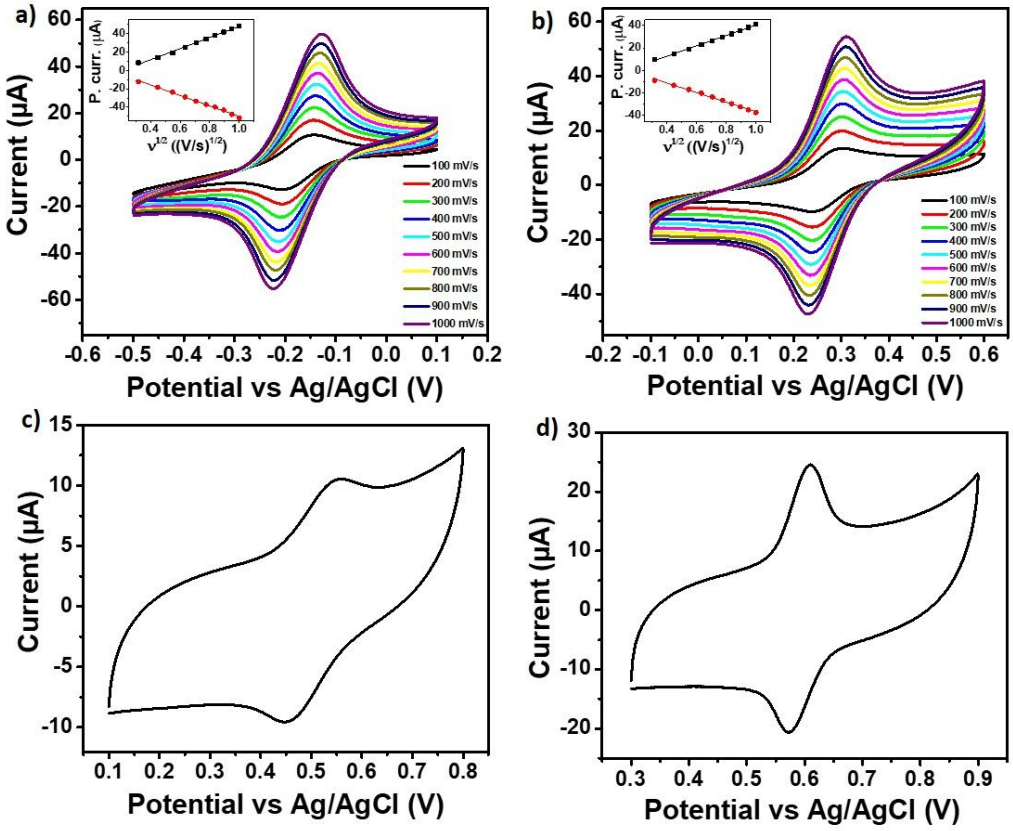

Figure 3. Cyclic voltammograms for four redox systems at graphitic carbon electrodes: a) 1.0 mM $[Ru(NH_3)_6]^{3+/2+}$ in 1 M KCl. Inset: peak oxidation and reduction values *vs* square root of potential scan rate; b) 1 mM $[Fe(CN)_6]^{3-/4-}$ in 1 M KCl. Inset: peak oxidation and reduction values *vs* square root of potential scan rate; c) 1 mM $Fe^{2+/3+}$ in 0.1 M $HClO_4$; d) 1 mM DA in 0.1 M $HClO_4$.

Further characterization was performed with the inner sphere $[Fe(CN)_6]^{3-/4-}$, a redox couple sensitive to the electrode microstructure and for which the HET process is known to depend strongly on the density of exposed edge plane sites.[1] Figure 3b shows that electrodes display fast electron transfer rates for $[Fe(CN)_6]^{3-/4-}$. The formal potential for this couple was 0.271 V. The average ΔE_p calculated over three samples at 100 mV/s scan rate was 61 mV (σ = 5.1 mV). The value of k^0_{app} was calculated as 1.3×10^{-1} cm/s, as determined by the Nicholson method (further details in Figure S2b). This k^0_{app} value was 10 times higher than the value previously obtained by our group for graphitic carbon electrodes obtained with 405 nm laser cutters. Interestingly, the morphological investigation of previous electrodes showed formation of porous graphitic carbon structures but not evidence of edge planes formation, in contrast with what reported for the present electrodes and therefore justifies the observed sharp increase of the HET process.[20] For this system the effect of scan rate on the peak current was also determined. A linear relationship between the peak oxidation/reduction current and the square root of the scan rate (inset of Figure 3b) was observed. The data recorded with this system indicate that the electrodes possess a surface structure capable of supporting

rapid electron transfer. The data correlates well with the morphology displayed in the SEM images (Figure 2a) showing a high density of exposed edge-planes at the electrode surface.

Figure 3c shows a CV recorded for $Fe^{3+/2+}$, another inner sphere redox system sensitive to surface carbon-oxygen functionalities, especially surface carbonyl groups, on sp^2 carbon electrodes.[1] ΔE_p for $Fe^{2+/3+}$ was 113 mV at a scan rate of 100 mV/s – giving a k^0_{app} value of 6.5×10^{-3} cm/s. This value is of the same order of magnitude as values reported for reduced graphene sheet films, and fast in comparison with glassy carbon electrodes.[36] The rapid electron-transfer in the $Fe^{2+/3+}$ reaction has been reported to be correlated to the presence of carboxyl and carbonyl surface groups and it is consistent with the findings of the XPS data (Figure 2d). Finally, Figure 3d shows CV of DA, a redox system which requires adsorption and is sensitive to the presence of oxides.[1, 36] At a scan rate of 100 mV/s the ΔE_p was 37 mV, much lower than values previously reported for glassy carbon electrodes and lower than the 60 mV value reported for reduced graphene sheets.[36]

In order to evaluate the electrochemical contribution of the high porosity/high surface area, a comparison between the electrode geometric and electrochemical areas was

carried out. At first glance the comparison between the geometric area of the electrode (1.72 mm^2, 0.215 mm width X 8 mm length, corresponding to the dimeter of the O-ring in the electrochemical cell) and the electrochemically active area (1.5 ± 0.3 mm^2, calculated by the Randles-Sevcik equation) suggested no contribution arising from the porous morphology of the electrode.[37] However, closer investigation of the electrochemical behaviour of the fabricated electrodes showed that the full area of the electrodes exposed to the analyte solution was not entirely electrochemically active. A large resistance (2.1 kΩ ± 0.08) was measured across these electrodes, from end-to-end, creating a potential-drop across the electrode upon current passage. This suggested that the entire electrode was not equipotential and that much of the area furthest away from the potentiostat connection did not reach a potential allowing it to contribute to the electrochemical reaction. This is similar to behaviour previously reported in the use of Au nanowire electrodes.[38] Further investigation showed that this potential-drop became insignificant at electrode lengths of between ¼ and ½ of the 8 mm electrochemical cell diameter. For such electrodes, as shown in Figure 4, the ratio between calculated geometric area and electrochemically active area raised to 1.63 and 1.23 for ½ and ¼ electrodes,

respectively, compared to 0.87 for the full sized electrode (see further details in Figure S3,a). This data showed that the contribution from the increased surface area arising from the porous morphology did have significant contribution for shortened electrodes, whereby the entire electrode surface was electrochemically active.

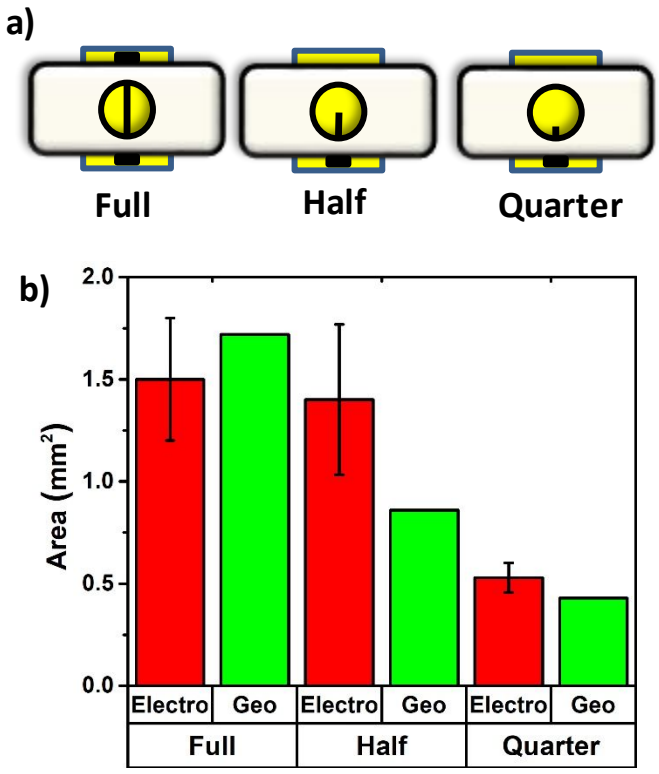

Figure 4. (a) Schematic of the Full, Half, and Quarter electrodes; (b) Comparison between the geometric area and electrochemically active area of electrodes calculated at 100 mV/s.

Further investigation of the effect of the potential-drop across the electrode was conducted by connecting the potentiostat to both ends of the electrode simultaneously, and shortening the length of the electrode by splitting it into two halves (see schematic inset of Figure 5,a). The splitting of the electrode ensures that the geometrical area is less than that of the full electrode. Conductive silver paint was used to create a contact for the potentiostat at a single point for both electrodes, making both sides of the electrode equipotential (resistance of the silver paint length is < 5 Ω). Despite the slightly smaller area, the cyclic voltammetry performed in $Fe(CN)_6^{3-/4-}$ resulted in a much higher peak current for the split electrode, equal to 2.7 times that of the full electrode as clearly shown in Figure S5,a. Given the problems posed by the large electrical resistance of the single line (~200 μm thick) electrode, a wider electrode (3 mm) was produced with considerably lower resistance across its 18 mm length (96 Ω ± 4). An experiment similar to that with the full and split electrode was conducted to investigate if the lower resistance of such a design would render the effect of the potential-drop negligible. Conductive silver paint was used to create a single contact for both ends of the electrode ('short-circuit' design). The electrochemical responses of this setup were compared with those of the single

connection and are shown in Figure 5b,c. The short-circuit setup did not result in an enhanced current response. The same area was active in both cases. Hence, the smaller resistance allowed the entire electrode to contribute to the electrochemical reaction. The difference that should be noted is in the ΔE_P values of the two setups: for the "normal mode" the values were 111 mV and 113 mV, whereas for the short-circuit mode the values were 69 mV and 75 mV. While in the normal setup the entire electrode became active and contributed to the reaction, a small potential gradient across the electrode as the potential was scanned by the potentiostat led to a lag in the response, and a larger peak separation. Figure S5 displays the behaviour of both setups with increasing scan rate. While the short-circuit mode maintained perfect linearity between peak current and square root of scan rate (Figure S5,b inset) the normal setup lost linearity at scan rates higher than 0.5 V/s, as the potential gradient across the electrode became significant (Figure S5,a inset).

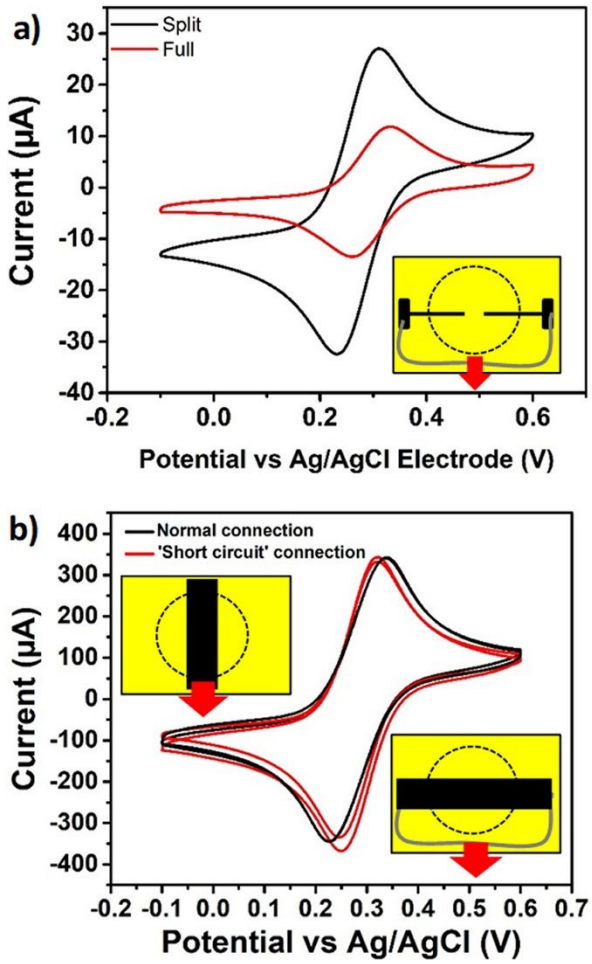

Figure 5. a) Cyclic voltammograms of Split electrode (red curve) and Full electrode (black curve) for 1 mM $[Fe(CN)_6]^{3-/4-}$ in 1 M KCl redox system, scan rate 100 mV/s. Inset: graphitic description of the Split electrode connection; b) cyclic voltammograms of 3 mm wide graphitic carbon electrodes for 1 mM $[Fe(CN)_6]^{3-/4-}$ in 1 M KCl redox system, scan rate 100 mV/s. Normal connection (black curves) and short circuit connection (red curves) at graphitic carbon electrodes: Inset: graphitic description of the two connections. Red

arrows indicate potentiostat connections, broken circle indicates o-ring position in electrochemical cell.

The results of the ET reactions of the above-mentioned redox couples investigated by CV are summarized in Table 2. As comparison also the electrochemical performance of our graphitic carbon electrodes against other carbon-based electrodes reported in literature is shown in Table 3. In each case, the electron-transfer kinetics and electrocatalytic properties were favourable in comparison with glassy carbon electrode values in literature, and comparable with values obtained at graphene electrodes fabricated via multi-step processes.[39,36,1] The fast HET kinetics were ascribed to the abundance of edge-planes and surface defects of the graphitic carbon electrodes, as observed in the SEM images and in the Raman spectra of the electrodes. Specifically, the abundance of kinks as well as the presence of surface oxides observed by XPS analysis can explain the high ET resulting from the high DOS near the Fermi level.

Table 2. Summary of electrode performance. k^o values were calculated using ν ranging from 100 mV/s to 1000 mV/s for $[Ru(NH3)_6]^{3+/2+}$ and $[Fe(CN)_6]^{3-/4}$; values for $Fe^{2+/3+}$ and DA were calculated at 100 mV/s.

Analyte	Supporting Electrolyte	ΔE (mV)	D (cm^2s^{-1})	k^0 (cms^{-1})
$Ru(NH_3)_6^{2+/3+}$	1 M KCl	57.3	6.5×10^{-6}	$6.93 \times 10^{-2} \pm 0.0014$
$[Fe(CN)_6]^{3-/4-}$	1 M KCl	60.7	7.63×10^{-6} (ox) 6.32×10^{-6} (red)	$1.26 \times 10^{-1} \pm 0.024$
$Fe^{2+/3+}$	0.1 M $HClO_4$	113	7.9×10^{-6}	6.53×10^{-3}
Dopamine	0.1 M $HClO_4$	37	6×10^{-6}	2.26×10^{-2}

Table 3. Summary of electrochemical performance for carbon-based electrodes obtained with $[Ru(NH3)_6]^{3+/2+}$ and $[Fe(CN)_6]^{3-/4-}$ mediators.

	ΔE_P (mV), $Ru(NH_3)_6^{2+/3+}$	ΔE_P (mV), $[Fe(CN)_6]^{3-/4-}$	k^0 (cms^{-1}), $Ru(NH_3)_6^{2+/3+}$	k^0 (cms^{-1}), $[Fe(CN)_6]^{3-/4-}$	Reference
450 nm laser scribed graphitic carbon	57.3	60.7	6.93×10^{-2}	1.26×10^{-1}	Present work
405 nm laser scribed graphitic carbon	74.5	85.6	1.46×10^{-2}	1.3×10^{-2}	[20]
Glassy Carbon	64	68	5.5×10^{-2}	2.9×10^{-2}	[32]
Reduced Graphene Sheet Films	61	65	1.8×10^{-1}	4.9×10^{-2}	[32]
HOPG basal plane			1.4×10^{-3}	$<10^{-7}$	[1]
HOPG edge plane			8.8×10^{-3}	0.06 – 0.1	[19, 1]
Laser scribed graphene (LSG)	95	85.6	$*8.7 \times 10^{-2}$	$*1.15 \times 10^{-1}$	[19]
Pt/LSG	74.5	70.8	$*2.3 \times 10^{-1}$	$*2.8 \times 10^{-1}$	[19]

*Suspected erroneously large k^0 calculation.

As reported above, graphitic carbon electrodes exhibited low peak to peak separations (<59 mV/*n*) for CV scans of standard redox couples $[Ru(NH_3)_6]^{2+/3+}$ and $[Fe(CN)_6]^{3-/4}$. Although it is common practice to define the electron transfer mechanism as diffusion limited process (following the semi-infinite planar diffusion model) and to attribute small voltammetric peak separations to enhanced electrocatalytic properties of the electrode material, other contributing factors could be at play in highly porous 3D systems. For example, it was reported that in glassy carbon-modified single wall carbon nanotube (GC/SWCNT) electrodes the contribution from thin layer mass transport within the porous 3D networks was significant.[40] In such systems, the analyte penetrated the porous structures becoming trapped within the electrode pores. In such a scenario the resultant CV scans from the porous electrode were a combination of the expected semi-infinite planar diffusion model and a thin layer contribution. Thus, for such a system, calculating the kinetic constant k^0 by the Nicholson method would lead to an erroneously large value – with the lower peak separation being attributed to faster kinetics without accounting for the thin-layer contribution.

In order to examine the extent of such a contribution in our systems, an electrode was cycled in supporting electrolyte (KCl 1 M, 100 mV/s). After immersion in $[Fe(CN)_6]^{3-/4}$ (5 mM, 5 min, in 1 M KCl) followed by thorough rinsing in deionized water, the electrode was cycled again in supporting electrolyte. Data shown in Figure 6 demonstrate that the electrode was modified by simple immersion in the $[Fe(CN)_6]^{3-/4}$ solution. An oxidation/reduction peak formed as result of $[Fe(CN)_6]^{3-/4}$ being adsorbed on the electrode surface or trapped with the electrode porous network. We speculate that pockets of analyte solutions became trapped in between multiple layers of graphitic carbon structure, a process similar to the one reported by Streeter *et al.* for GC electrodes surface modified with single-walled carbon nanotubes (SWCNTs).[40] However, as shown in the insets of figure 3 (a) and (b), i_P for $[Ru(NH_3)_6]$ and $([Fe(CN)_6]$ was found proportional to the square root of the scan rate, as predicted by the Randles-Sevcik equation for quasi-reversible reactions at electrodes governed by semi-infinite linear diffusion. Instead, for processes governed by thin layer diffusional processes, i_P would be proportional to the scan rate.[41] Evidently for the graphitic carbon electrodes in this study there is a contribution from immobilised solution within the porous electrode, but not significant enough to perturb the

response from being interpreted as semi-linear diffusion. Hence, the lower peak separations can indeed be attributed to the excellent electrocatalytic properties of the graphitic carbon electrode.

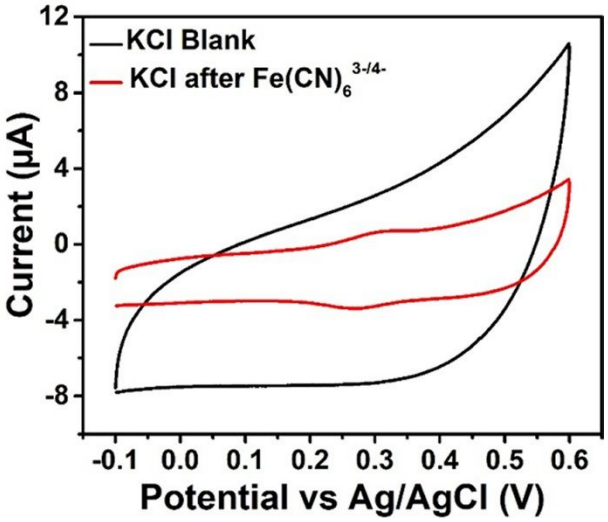

Figure 6. CV of supporting electrolyte KCl 0.1 M in PBS 0.1 M (pH = 7.4) (back curve) and CV of KCl obtained after cycling the electrode in $Fe(CN)_6^{3-/4-}$ 0.1 M (red curve). Scan rate 100 mV/s.

Biosensor performance

Given the excellent electrocatalytic and electron transfer properties of the graphitic carbon electrode its performance as biosensor was investigated. In order to evaluate the sensitivity and selectivity of the graphitic carbon electrodes it was decided to study their

electrochemistry toward a DA, UA and AA system. As well as the specific importance of each specie as biomarker for human health monitoring, DA, UA and AA coexist in the central nervous system and their electrochemical oxidation peaks overlap in conventional solid electrodes, making difficult to perform individual sensing. Therefore, the purpose of the investigation was to demonstrate the ability of graphitic carbon electrodes to differentiate DA, UA and AA species by providing enhanced separation of oxidation potentials. Figure 7a shows a CV scan of a solution containing a mixture of DA (1 mM), UA (1 mM) and AA (1 mM) in 0.1 M PBS recorded at 100 mV/s. Individual DA (1 mM), UA (1 mM) and AA (1 mM) in 0.1 M PBS CVs are shown in Figure S4. The curve shows well defined oxidation peaks at 0.044 V, 0.218 V, and 0.389 V corresponding to the oxidation of AA, DA and UA, respectively. The resulting oxidation peak separations were: $\Delta E_{AA\text{-}DA}$ = 0.174 V, $\Delta E_{DA\text{-}UA}$ = 0.171 V and $\Delta E_{AA\text{-}UA}$ = 0.345 V, showing capability for selective determinations of individual species. Figure 7b shows a DPV scan for the same system, displaying excellent resolution of the three peaks for AA, DA and UA. The peak separation values are as follows: $\Delta E_{AA\text{-}DA}$ = 0.184 V, $\Delta E_{DA\text{-}UA}$ = 0.160 V and $\Delta E_{AA\text{-}UA}$ = 0.344 V, allowing easy identification of concomitant species. These values are lower than

those reported in literature for graphene-based electrodes and comparable to values reported for graphitic carbon electrodes with enhanced catalytic activity, obtained by post-fabrication Pt or PEDOT electrodeposition steps (see Table S2 for further details).[19, 24] The graphitic carbon electrode material displayed high selectivity due to a combination of enhanced electron transfer associated to its porous morphology, the enhanced catalytic activity arising from its edge-plane-rich structure and surface functional groups, and the easy access to biomolecules provided by its extended 3D porous network morphology. This is encouraging for the potential of graphitic carbon fabricated with low-cost, low-powered laser systems to be used as a cheap and easily-fabricated biosensing material.

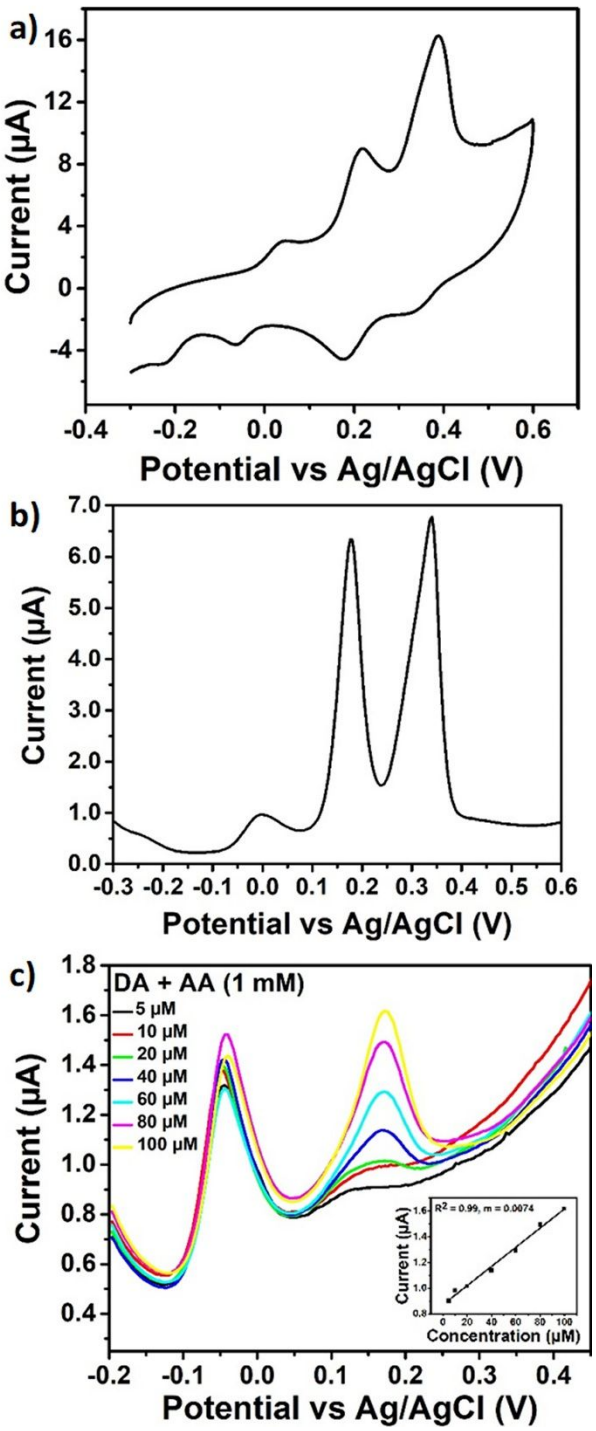

Figure 7. CV (a) and DPV (b) curves for AA, DA and UA 1 mM in 0.1 M PBS (pH = 7.4); c) DPV response of different concentrations of DA in presence of AA 1 mM in PBS 0.1 M

(pH = 7.4). Scan rate 100 mV/s. Inset: concentration vs current linear response for DA calculated from DPV curves shown in 7,b.

Figure 7c shows the DPV response of varying concentrations of DA (5 μM – 100 μM) in the presence of a constant concentration of AA (1 mM). The oxidation peak current at 0.172 V associated to DA increased as its concentration was increased from 5 μM to 100 μM. In contrast the oxidation peak current at -0.44 V associated to AA remained almost constant, showing again the electrode good speciation ability between potentially interfering species. As shown in the inset of Figure 6c, the current response to DA concentration was linear in the range of 5-100 μM, with a sensitivity of 0.0074 A/M. The sensitivity parameter was calculated from the slope of the calibration plot. A comparison of the presented graphitic carbon electrode with similar graphitic carbon structures is reported in Table S2. However, the limit of detection for DA concentration was equal to only 300 μM. This unexpectedly high value was attributed to low current response across the electrodes. However, with the previously discussed low resistance 3 mm wide

electrodes a substantial improvement in the biosensor performance was observed, resulting in calculated LODs of 5.5 μM for dopamine (see Figure S6).

The performance of our electrode was comparable to those of graphitic carbon electrodes fabricated with high power CO_2 lasers and with electrocalytic properties enhanced by post-fabrication treatments such as Pt or PEDOT deposition. In contrast the presented electrodes were fabricated with low cost/low power visible hobbyist lasers and were used without any post-fabrication enhancement step. Furthermore, comparison pf performance with previously reported electrodes fabricated by 405 nm laser irradiation[20] showed superior sensitivity for DA and superior speciation capabilities for DA, AA and UR mixtures (see Figure S7). The developed electrochemical setup was also compatible with light weight portable instrumentation. This setup is shown in Figure S8. Also shown is a CV of $[Fe(CN)]^{3-/4-}$ recorded with a handheld potentiostat. The peak separation and peak current is in agreement with the results obtained using the bench bi-potentiostat. Therefore, these results are very encouraging for the development of low cost routes for fabrication of disposable and sensitive biosensors.

Conclusions

Graphitic carbon electrodes were readily fabricated by a direct laser writing method by using a low-cost hobbyist laser with 450 nm laser illumination. The electrodes displayed a highly porous and 3D structure, rich in defects and edge planes which was conducive to good electrochemical sensing capabilities. The HET kinetics were characterised by the use of outer sphere $[Ru(NH3)_6]^{3+/2+}$ and inner sphere $[Fe(CN)_6]^{3-/4-}$, $Fe^{2+/3+}$ and DA revealing a diffusion-controlled quasi-reversible electron transfer at the electrode surface. Overall, better electrochemical performance was obtained compared to other graphitic carbon electrodes fabricated either by visible or infrared laser illumination. The superior electrocatalytic performance was ascribed to the formation of highly porous and 3D structures, characterised by high surface area, large networks and abundance of defect and edge planes and facilitating analyte adsorption and circulation. The effect of porosity on the ET kinetics was assessed by comparison between geometric area and electrochemically active area. Also, the contribution of other mechanisms such thin layer diffusion mechanisms was taken in consideration in order to clarify the origin of the enhanced electrocatalytic effect observed in these electrodes. However, such contribution was considered to be too small to perturb the dominant diffusion limited

process. Finally, the fabricated graphitic carbon electrodes showed excellent biosensing performance and were able to perform electrochemical detection of AA, DA and UA in solution without further electrode modification and by both CV and DPV methods. This in-depth study shows that direct laser writing techniques constitute a viable route for the fabrication of low-cost disposable electrochemical biosensing platforms for in-field, point-of-care and lab-on-a-chip applications, as well as in other integrated bioelectronics applications.

ASSOCIATED CONTENT

Supporting Information. XPS data; Heterogeneous Electron Transfer (HET) coefficient rate calculations; peak current intensity and electrochemical active area; cyclic voltammetry of ascorbic acid, dopamine and uric acid; electrochemical characterization wider graphitic carbon electrodes (3 mm); dopamine detection with wider graphitic carbon electrodes (3 mm); comparison biosensor performance with other graphitic carbon electrodes; electrochemical setup and portable potentiostat measurement.

AUTHOR INFORMATION

Corresponding Author

*daniela.iacopino@tyndall.ie

Author Contributions

The manuscript was written through contributions of all authors. All authors have given approval to the final version of the manuscript.

Funding Sources

This publication has emanated from research conducted with the financial support of the European Union H2020 project Apache (814496) project, Science Foundation Ireland (SFI) and the Department of Agriculture, Food and Marine on behalf of the Government of Ireland under Grant Number 16/RC/3918, 16/RC/3835and SFI TIDA 5118, co-funded by the European Regional Development Fund.

REFERENCES

1. McCreery, R. L. Advanced Carbon Electrode Materials for Molecular Electrochemistry. *Chem. Rev.* **2008**, 108, 2646-2687.

2. Wang, J. *Analytical Electrochemistry*, 2nd *ed.* Wiley, New York, NJ, **2000**

3. Szuneritis, S.; Boukherroub, R. Graphene-based Biosensors, *Interface Focus*, **2018,** 8, 20160132.

4. Shao, Y; Wang, J.; Wu, J.; Aksay, I. A.; Lin, Y. Graphene Based Electrochemical Sensors and Biosensors: A review. *Electroanalysis*, **2010,** 22 (10), 1027-1036.

5. Unwin, P. R.; Güell, A. G.; Zhang, G. Nanoscale Electrochemistry of sp2 Carbon Materials: from Graphite and Graphene to Carbon Nanotubes. *Acc. Chem. Res*. **2016**, 49, 2041−2048.

6. Chen, D.; Feng, H.; Li, J. Graphene Oxide: Preparation, Functionalization, and Electrochemical Applications. *Chem. Rev*. **2012**, 112, 6027−6053.

7. Wu, Z.-S.; Sun, Y.; Tan, Y.-Z.; Yang, S.; Feng, X.; Müllen, K. Three-Dimensional Graphene-Based Macro- and Mesoporous Frameworks for High-Performance Electrochemical Capacitive Energy Storage. *J. Am. Chem. Soc.* **2012**, 134, 19532−19535.

8. Wu, M.; Meng, S.; Wang, Q.; Si, W.; Huang, W.; Dong, X. Nickel−Cobalt Oxide Decorated Three-Dimensional Graphene as an Enzyme Mimic for Glucose and Calcium Detection. *ACS Appl. Mater. Interfaces*, **2015**, 7, 21089−21094.

9. Chen, Z.; Ren, W.; Gao, L.; Liu, B.; Pei, S.; Cheng, H.-M. Three-Dimensional Flexible and Conductive Interconnected Graphene Networks Grown by Chemical Vapour Deposition. *Nat. Mater.* **2011**, 10, 424−428.

10. Amal Raj, M.; Abraham John, S. Fabrication of Electrochemically Reduced Graphene Oxide Films on Glassy Carbon Electrode by Self-Assembly Method and Their Electrocatalytic Application. *J. Phys. Chem. C* **2013**, 117, 4326−4335.

11. Lawes, S.; Riese, A.; Sun, Q.; Cheng, N.; Sun. X. Printing nanostructured carbon for energy storage and conversion applications. *Carbon* **2015**, 92, 150-176.

12. Korhonen, H.; Sinh, L. H..; Luog, N. D.; Lehtinen, P.; Verho, T.; Partanen, J.; Seppälä, J. Fabrication of graphene-based 3D structures by stereolithography. *Phys. Status Solidi A* **2015**, 213, 982-985.

13. Da Costa, T. H., Song, E.; Tortorich, R. P.; Choi, J. W. A paper-based electrochemical sensor using inkjet-printed carbon nanotube electrodes, *ECS J Sol State Sci technol*. **2015,** 4 (10) S3044-S3047.

14. Das, S. R.; Nian, Q.; Cargill, A. A.; Saei, M.; Cheng, G. J.; Calussen, J. C. 3D nanostructured inkjet printed graphene via UV-pulsed laser irradiation enables paper-based electronics and electrochemical devices. *Nanoscale*, **2016**, 8, 15870—15879

15. Griffiths, K.; Dale, C. Hedley, J.; Kowal, M. D.; Kaner, R. B.; Keegan, N. Laser-scribed graphene presents an opportunity to print a new generation of disposable electrochemical sensors. *Nanoscale*, **2014**, 6, 13613—13622

16. Strong, V.; Dubin, S.; El-Kady, M. F.; Lech, A.; Wang, Y.; Weiller, B. H.; Kaner, R. B. Patterning and electronic tuning of laser scribed graphene for flexible all-carbon devices. *ACS Nano*, **2012** 6(2), 1395-1403.

17. Ye, R. James, D. K.; Tour, J. M. Laser-Induced Graphene. *Acc chem res*, **2018**, 51, 1609-1920

18. Lin, J.; Peng, Z.; Liu, Y.; Zepeda, F.; Ye, R.; Samuel, E. L. G.; Yacamn, M. J.; Yakobson, B. I.; Tour, J. M. Laser-induced graphene films from commercial polymers. *Nature Commun.* **2014,** 5, 5714.

19. Nayak, P.; Kurra, N.; Xia, C; Alshareef, H. Highly efficient laser scribed graphene electrodes for on-chip electrochemical sensing applications. *Adv. Electron. Mater*. **2016**, 2, 1600185.

20. Burke, M.; Larrigy, C.; Vaughan, E.; Paterakis, G.; Sygellou, L.; Quinn, A. J.; Herzog, G.; Galiotis, C., Iacopino D. Fabrication and electrochemical properties of three dimensional porous graphitic electrodes obtained by low-cost laser induced graphene (LIG). *ACS Omega*, **2020**, 5, 1540−1548.

21. Yen, G. C.; Duh, P. D.; Tsai, H. L. Antioxidant and pro-oxidant properties of ascorbic acid and gallic acid. *Food Chem.* **2002**, 79, 307-313.

22. Liu, Q.; Zhu, X.; Huo, Z.; He, X.; Liang, Y.; Xu, M. Electrochemical detection of dopamine in the presence of ascorbic acid using PVP/graphene modified electrodes. *Talanta*, **2012**, 97, 557-562.

23. Hou, T.; Gai, P.; Song, M.; Zhang, S.; Li, F.; Synthesis of three-layered SiO2@Au nanoparticles@polyaniline nanocomposite and its application in simultaneous electrochemical detection of uric acid and ascorbic acid. *J Mater. Chem. B.* **2016**, 13, 2314-2321.

24. Xu, G.; Jarjes, Z; Desprez, V; Kilmartin, P; Travas-Sejdic, J. Sensitive, selective, disposable electrochemical dopamine sensor based on PEDOT-modified laser scribed graphene. *Biosens. Bioelectr.* **2018**,107 184-191.

25. Nicholson, R. S. Theory and Application of Cyclic Voltammetry for Measurement of Electrode Kinetics. *Anal. Chem.* **1965**, 37, 1351-1355.

26. Romero, F. J.; Salinas-Castillo, A.; Rivadeneyra, A.; Albrecht, A.; Godoy, A.; Morales, D. P.; Rodriguez, N. In-Depth Study of Laser Diode Ablation of Kapton Polyimide for Flexible Conductive Substrates. *Nanomaterials*. **2018**, 8, 517-528.

27. Zhang, Z.; Song, M.; Hao, J.; Wu, K.; Li, C.; Hu, C; Visible light laser-induced graphene from phenolic resin: A new approach for directly writing graphene-based electrochemical devices on various substrates. *Carbon* **2018**, 127, 287-296.

28. Ferrari, A. C.; Basko, D. M. Raman spectroscopy as a versatile tool for studying the properties of graphene. *Nat. Nanotechnol*. **2013**, 8, 235-246.

29. Lespade, P.; Al-Jishi, R.; Dresselhaus, M. S. Model for Raman scattering from incompletely graphitized carbons. *Carbon* **1982**, 20, 427-431. 27

30. Nemanich, R. J.; Glass, J. T.; Lucovsky, G.; Shroder, R. E. Raman scattering characterization of carbon bonding in diamond and diamondlike thin films. *J. Vac. Sci. Technol. A: Vacuum, Surfaces, Film.* **1988**, 6, 1783-1787.

31. Eckmann, A.; Felten, A.; Mishchenko, A.; Britnell, L.; Krupke, R.; Novoselov, K. S.; Casiraghi, C. Probing the nature of defects in graphene by Raman Spectroscopy. *Nano Lett.* **2012**, 12, 3925-3930.

32. Yuan, B.; Zeng, X.; Xu, C.; Liu, L.; Zhang, D.; Fan, Y. Electrochemical modification of graphene oxide bearing different types of oxygen functional species for the electro-catalytic oxidation of reduced glutathione*. Sens. Act. B: Chemical.* **2013,** 184, 15-20.

33. Stergiu. D. V.; Diamanti, E. K.; Gournis, D.; Prodomis, M. I. Comparative study of the different types of graphenes as electrocatalysts for ascorbic acid. *Electrochem. Comm*. **2010,** 12 (10), 1307-1309.

34. Fisher, A. E.; Show. F.; Swain, M. Electrochemical Performance of Diamond Thin-Film Electrodes from Different Commercial Sources. *Anal Chem*. **2004**, 74, 2553-2560.

35. Chen, P.; McCreery, R. L. Control of Electron Transfer Kinetics at Glassy Carbon Electrodes by Specific Surface Modification. *Anal Chem.* **1996**, 68, 3958-3965.

36. Tang, L.; Wang, Y.; Li, Y.; Feng, H.; Li, L.; Li, J. Preparation, structure, and electrochemical properties of reduced graphene sheet films. *Adv Funct. Mater*. **2009**, 19, 2782-2789

37. Bard, A. J.; Faulkner, L. R.; Electrochemical Methods, 2nd ed. John Wiley &sons, New York, **2010**.

38. Muratova, I. S.; Mikhelson, K. N.; Ermolenko, Yu.; Offenhäusser, A.; Mourzina, Yu. On “resistance overpotential” caused by a potential drop along the ultrathin high aspect ratio gold nanowire electrodes in cyclic voltammetry. *J Solid State Electrochem,* **2016**, 20, 3359-3365.

39. Yu, B.; Kuang, D.; Liu, S.; Liu, C.; Zhang, T. Template-assisted self-assembly method to prepare three-dimensional reduced graphene oxide for dopamine sensing. *Sensors and Actuators B,* **2015**, 205, 120-126.

40. Streeter, I.; Wildgoose, G. G.; Shao, L.; Compton, R. G. Cyclic voltammetry on electrode surfaces covered with porous layers: An analysis of electron transfer kinetics at single-walled carbon nanotubes modified electrodes. *Sens. Act. B: Chemical*,**2008,** 133, 462-466

41. Bard, A. J.; Faulkner, L. R. Electrochemical methods: Fundamentals and Applications, 2nd ed, Wiley: New York, **2001**, chapter 11, sect 7.

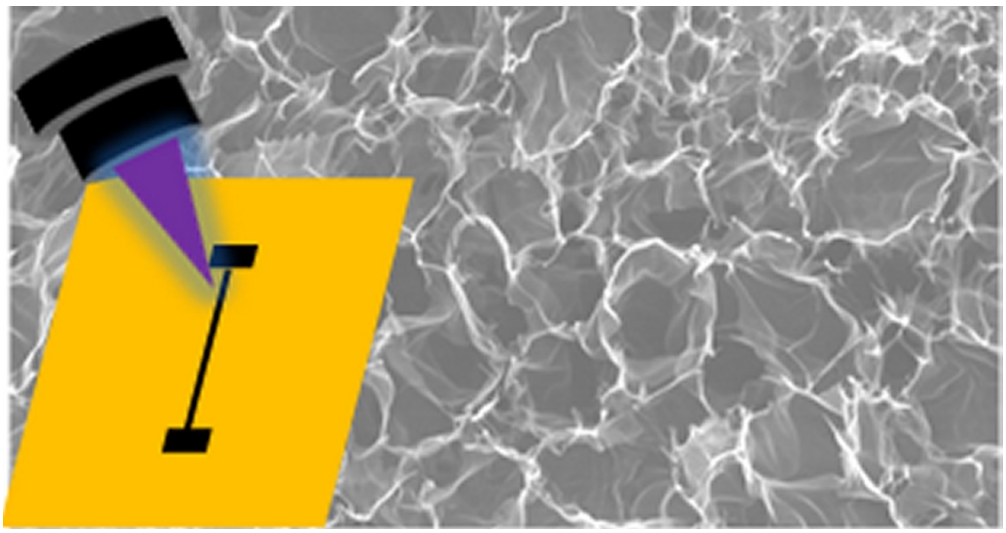

82x43mm (600 x 600 DPI)